High pressure thermoelasticity and sound velocities of Fe-Ni-Si alloys: Supplementary Material

Rachel A. Morrison[a,b,*], Jennifer M. Jackson[a,*], Wolfgang Sturhahn[a], Jiyong Zhao[c], Thomas S. Toellner[c]

[a] *Seismological Laboratory, California Institute of Technology, Pasadena, California, USA.*
[b] *ExxonMobil Upstream Integrated Solutions, Spring, Texas, USA.*
[c] *Advanced Photon Source, Argonne National Laboratory, Argonne, Illinois, USA.*

Contents

*Corresponding author
Email addresses: rachel.a.morrison@exxonmobil.com (Rachel A. Morrison), jackson@gps.caltech.edu (Jennifer M. Jackson)

1. Raw NRIXS spectra

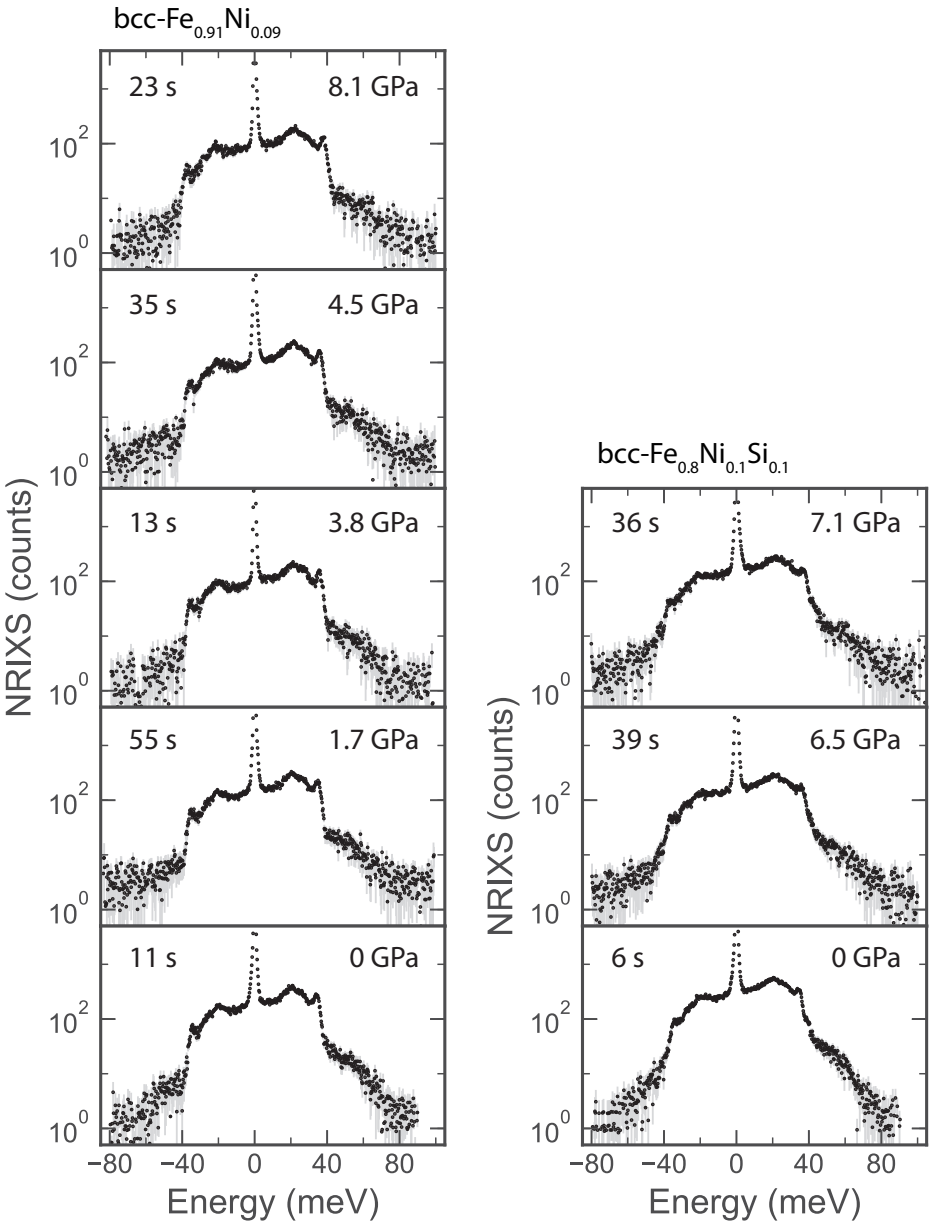

Figure S1: Raw (unnormalized) NRIXS spectra for bcc-$Fe_{0.91}Ni_{0.09}$ and $Fe_{0.8}Ni_{0.1}Si_{0.1}$ at 300 K collected around the resonance energy of ^{57}Fe at 14.5125 keV with a step size of 0.25 meV. We note that the NRIXS spectra of bcc-Fe is not displayed here and is plotted in Figure 1 in the main text. The numbers in the upper left of each panel indicate the collection time per data point.

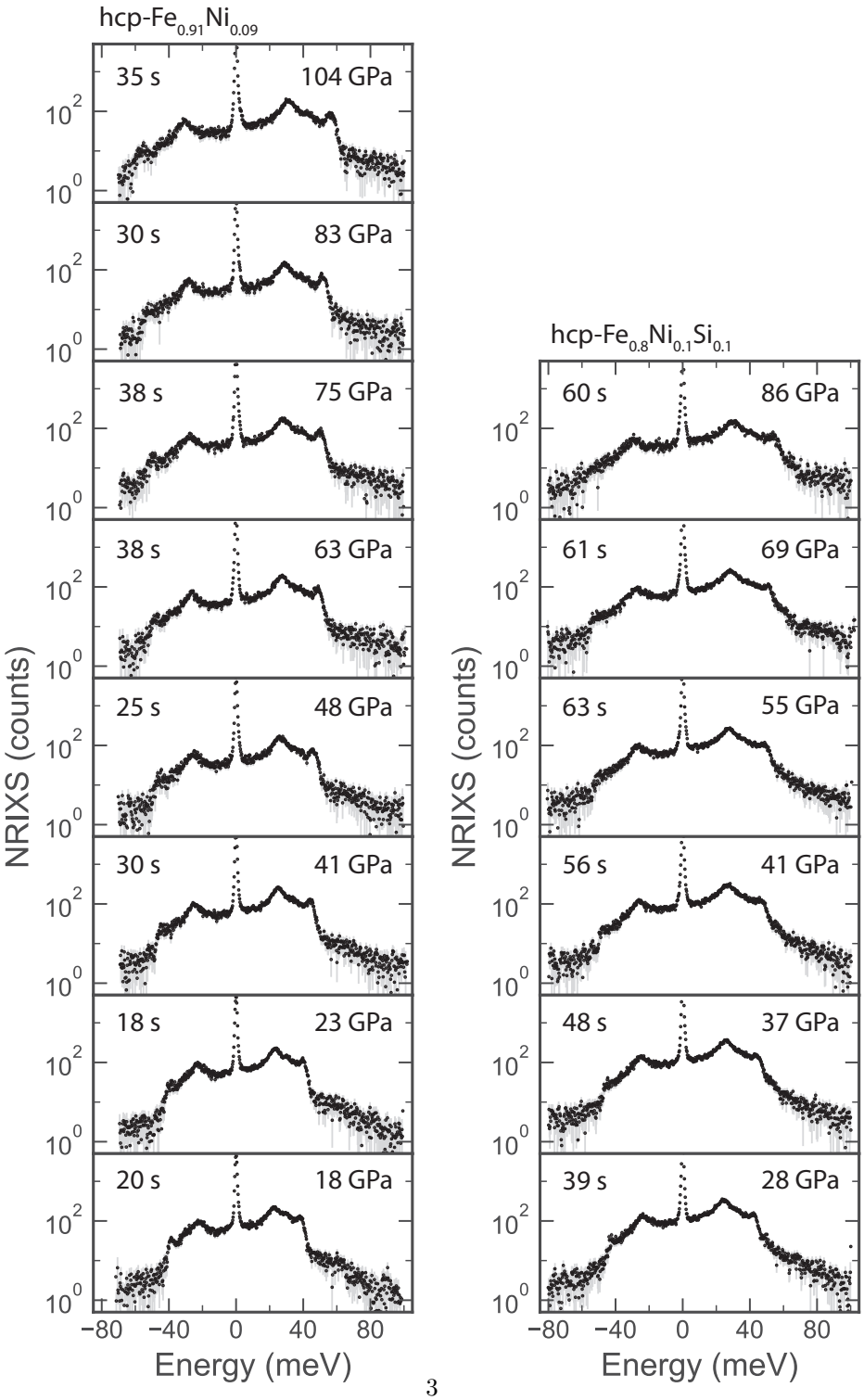

Figure S2: Raw (unnormalized) NRIXS spectra for hcp-$Fe_{0.91}Ni_{0.09}$ and $Fe_{0.8}Ni_{0.1}Si_{0.1}$ at 300 K collected around the resonance energy of ^{57}Fe at 14.5125 keV with a step size of 0.25 meV. The numbers in the upper left of each panel indicate the collection time per data point.

2. Vibrational Grüneisen parameter: Additional figures

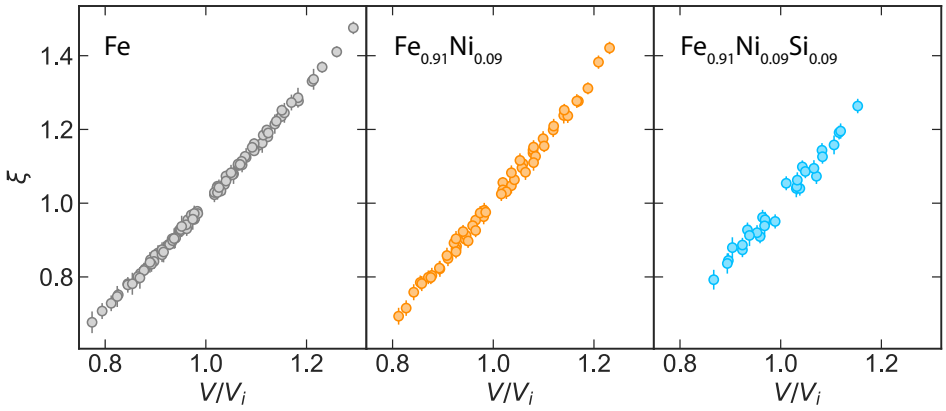

Figure S3: Phonon DOS scaling parameters for hcp-$Fe_{0.91}Ni_{0.09}$, $Fe_{0.8}Ni_{0.1}Si_{0.1}$, and Fe as determined from equation 12 and the procedure detailed in section 4 in the main text. Data for hcp-Fe is re-analyzed from *Murphy et al.* (2011a).

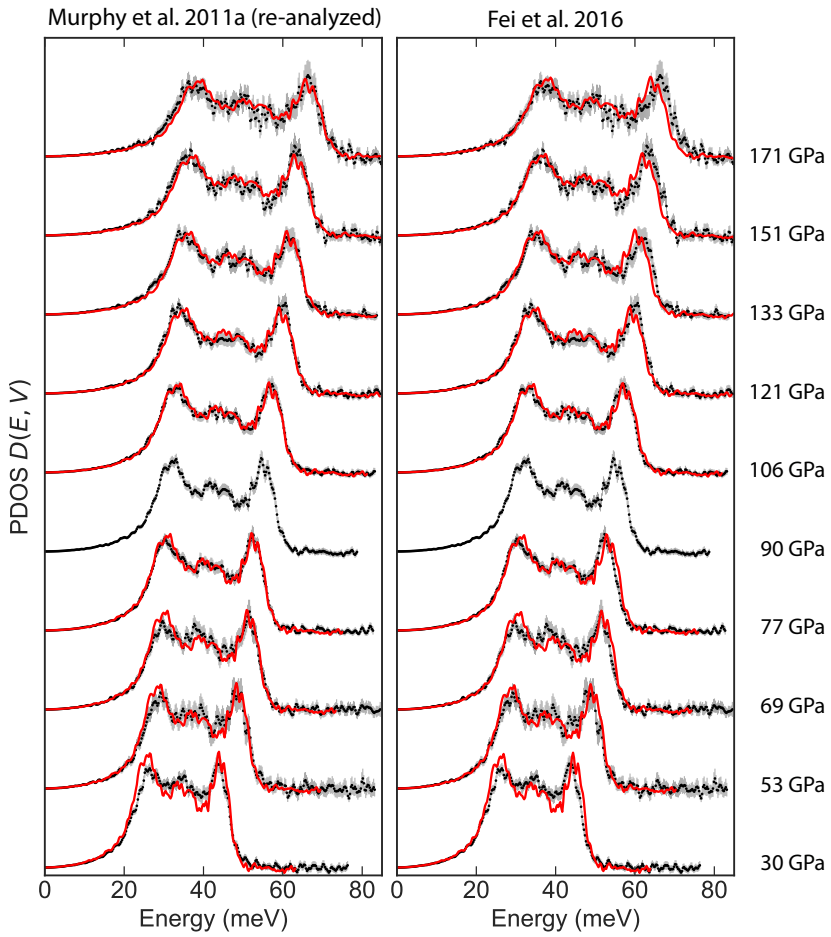

Figure S4: Scaled phonon DOSs (red) compared to measured phonon DOS (black with gray error bars) for hcp-structured Fe. The hcp-Fe phonon DOS at 90 GPa is scaled to each compression point according to equation 12. On the left is our analysis of *Murphy et al.* (2011a), and on the right is the phonon DOS scaling calculated from γ_{vib} from *Fei et al.* (2016).

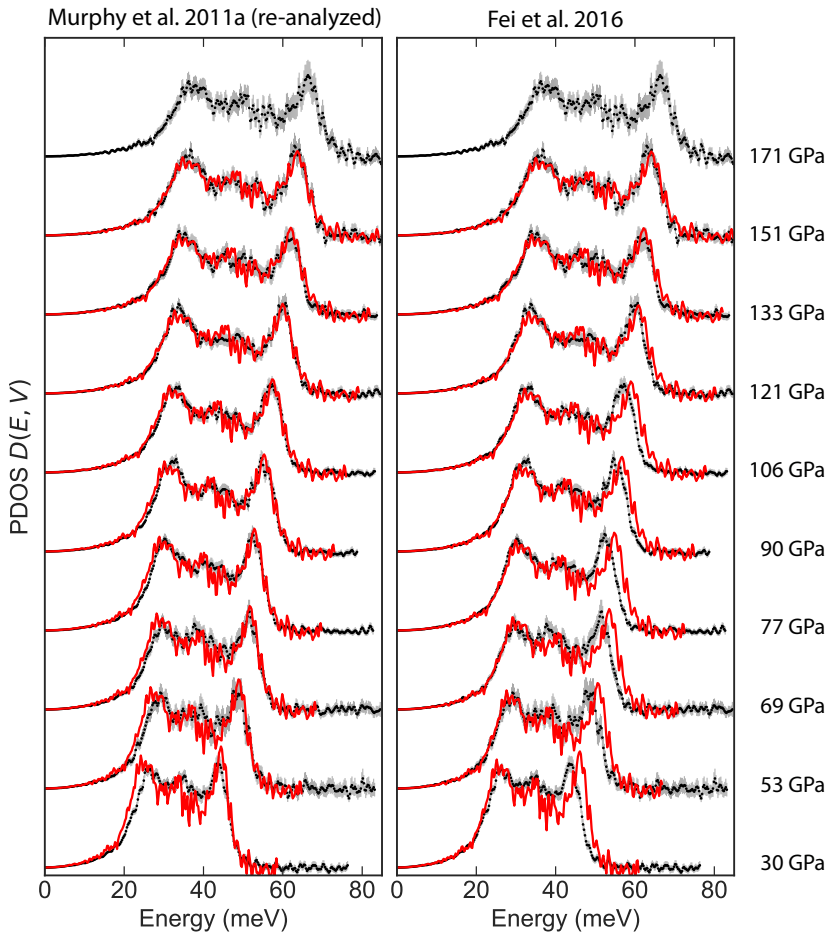

Figure S5: Scaled phonon DOSs (red) compared to measured phonon DOS (black with gray error bars) for hcp-structured Fe. The hcp-Fe phonon DOS at 171 GPa is scaled to each compression point according to equation 12. On the left is our analysis of *Murphy et al.* (2011a), and on the right is the phonon DOS scaling calculated from γ_{vib} from *Fei et al.* (2016).

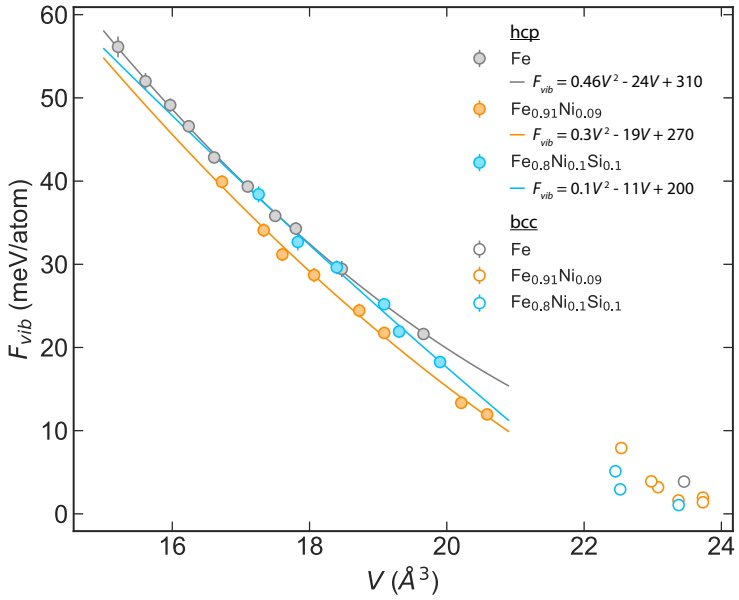

Figure S6: Harmonic vibrational free energy F^h_{vib} for $Fe_{0.91}Ni_{0.09}$, $Fe_{0.8}Ni_{0.1}Si_{0.1}$, and Fe at 300 K as determined from the phonon DOS. The hcp-Fe data is a re-analysis of data from *Murphy et al.* (2011b). Error bars where not shown are smaller than the symbols. Empirical equations for the hcp-phases are displayed.

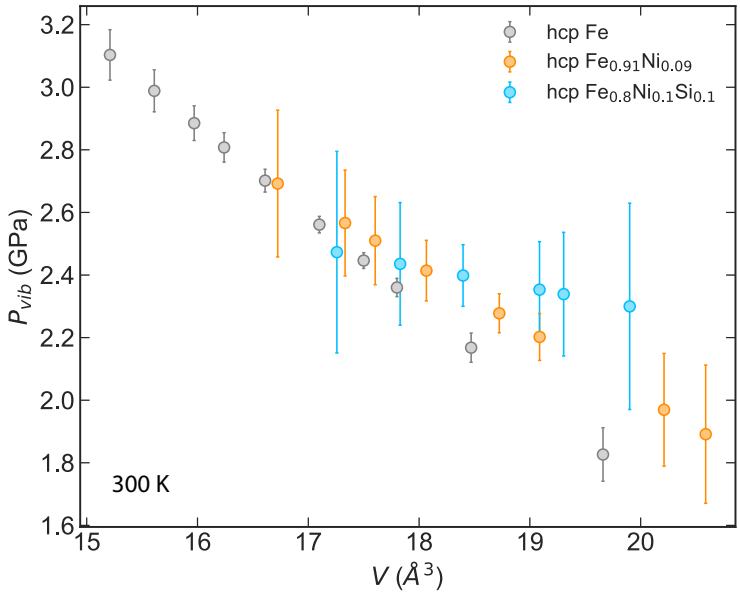

Figure S7: Harmonic vibrational thermal pressure P^h_{vib} for $Fe_{0.91}Ni_{0.09}$, $Fe_{0.8}Ni_{0.1}Si_{0.1}$, and Fe at 300 K as determined from the derivative of F^h_{vib}. The hcp-Fe data is a re-analysis of data from *Murphy et al.* (2011b).

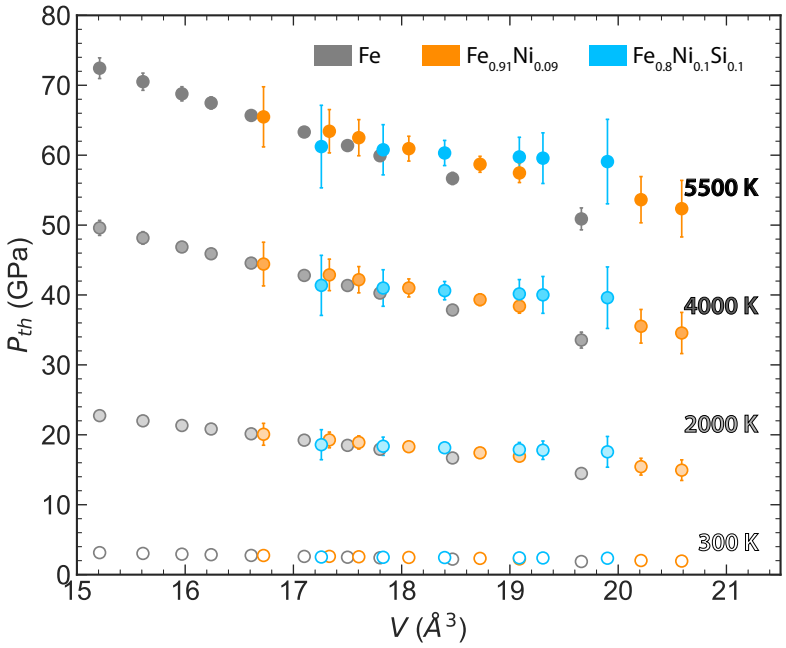

Figure S8: Thermal pressure P_{th} as a function of volume and temperature for hcp-$Fe_{0.91}Ni_{0.09}$, $Fe_{0.8}Ni_{0.1}Si_{0.1}$, and Fe. The hcp-Fe data is a re-analysis of data from *Murphy et al.* (2011b). We include harmonic, anharmonic, and electronic contributions to P_{th}. See text for more details.

3. An approximation for the vibrational Grüneisen parameter via an alternate determination method

To test the robustness and validity of the vibrational Grüneisen parameter determination method outlined in Section 4 of the main text, we approximate the vibrational Grüneisen parameter using a second method which does not require the application of the empirical equations 14 and 16 discussed in the main text. The scaling parameter ξ can be expressed as a relation between phonon branch energies at different volumes V and V_i, where V_i is the reference volume,

$$\xi = E_i/E. \tag{S1}$$

Equation 11 from the main text can then be coarsely approximated as

$$\gamma_{vib,i} \approx -\frac{V_i}{E_i}\left(\frac{E - E_i}{V - V_i}\right). \tag{S2}$$

Substituting equation S1 into equation S2, we find

$$\gamma_{vib,i} \approx -\frac{V_i}{E_i}\left(\frac{(E_i/\xi) - E_i}{V - V_i}\right) \approx \frac{(1 - 1/\xi)V_i}{V - V_i}. \tag{S3}$$

We select a single hcp phonon DOS collected at volume V_i to serve as a reference, and we pair it with each other phonon DOS of the same composition (at volume V) to estimate the corresponding $\gamma_{vib,i}$. We then average all estimated $\gamma_{vib,i}$ for a given reference phonon DOS. We repeat this process with each phonon DOS serving as a reference. While this method is an approximation for $\gamma_{vib,i}$, we note that it does not rely on the application of the empirical relation in equation 14 from the main text, on a linear least squares fit, or on fixing the fitting parameter q. Therefore, it can serve a check of the validity of equation 17 in the main text.

The two methods of determining $\gamma_{vib,i}$ agree well within error bars within the measured volume region. However, the $\gamma_{vib,i}$ curve calculated with equation 17 in the main text has a powerful advantage, as it can be extrapolated to 0 GPa or to higher pressures. Additionally, the $\gamma_{vib,i}$ curve is more reliable, because the other method depends on a very rough approximation for the derivative in equation 11 in the main text. We note that the error bars of the $\gamma_{vib,i}$ curve (calculated with equation 17) are much smaller than those of the estimated $\gamma_{vib,i}$ (calculated with equation S3) due to the imposition of equation 14 from the main text and the lack of the rough approximation in equation S2.

4. Lamb-Mössbauer factor

The Lamb-Mössbauer factor (f_{LM}) is the probability for recoilless absorption. It contains information about the binding of the resonant nuclei (^{57}Fe in this study) in the lattice, and it therefore depends on composition, local structure, pressure, and temperature. In NRIXS data, it is the ratio of the elastic to total incoherent scattering. It takes a form similar to that of the Debye-Waller factor. While the Debye-Waller factor describes coherent, fast scattering events, f_{LM} describes slow scattering events such as

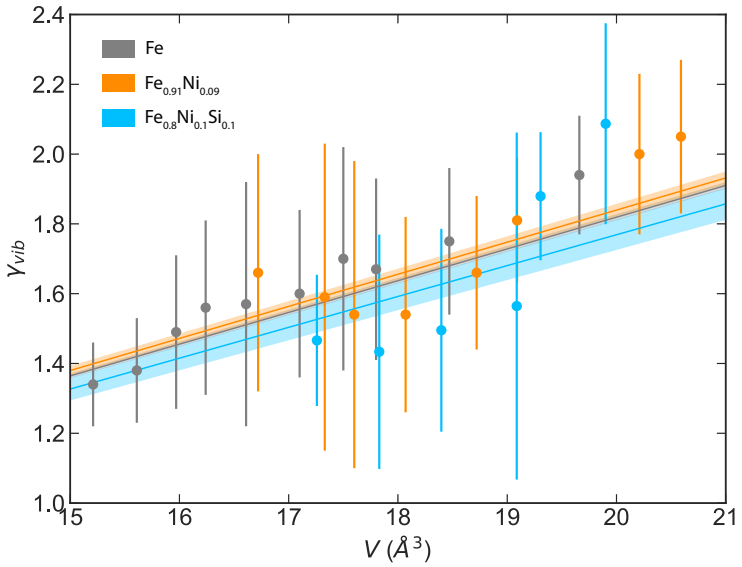

Figure S9: The vibrational Grüneisen parameter γ_{vib} for hcp-$Fe_{0.91}Ni_{0.09}$, $Fe_{0.8}Ni_{0.1}Si_{0.1}$, and Fe calculated using two methods. The hcp-Fe data is based on our re-analysis of data from *Murphy et al.* (2011a). The first method applies equation 17 from the main text (curves with shaded regions representing uncertainty). The second method applies equation S3 (filled circles) and is a rough approximation with larger uncertainties. It serves as a validity check on the assumptions of method 1, as it does not rely on the empirical relation of equation 14 in the main text.

those which take place over the lifetime of nuclear resonance (141 ns for ^{57}Fe) (*Sturhahn*, 2004).

There are typically two different methods of accessing f_{LM} from NRIXS measurements. First, f_{LM} can be determined from a moments analysis of the excitation probability density $S(E, V_i)$ (see Section 2 in the main text), where f_{LM} is related to the 0th-order moment $S_0(E, V_i)$ (*Sturhahn and Chumakov*, 1999). Second, f_{LM} can be calculated from the determined phonon DOS, which assumes a quasi-harmonic lattice model (see Section 2 in the main text). The quantity f_{LM} is related to the thermal motion of the resonant nuclei about their equilibrium positions, which can be quantified by the mean square atomic displacement $\langle u^2 \rangle$. From the phonon DOS, $\langle u^2 \rangle$ can be calculated as

$$\langle u^2 \rangle = \frac{E_R}{3k^2} \int \frac{1}{E} \coth \frac{\beta E}{2} D(E, V) dE, \tag{S4}$$

where k is the wavenumber of the resonant x-rays (k=7.306 Å^{-1} for ^{57}Fe). The Lamb-Mössbauer factor is then

$$f_{LM} = e^{-k^2 \langle u^2 \rangle}. \tag{S5}$$

We compare our determined f_{LM} from the moments analysis and the phonon DOS analysis for $Fe_{0.91}Ni_{0.09}$, $Fe_{0.8}Ni_{0.1}Si_{0.1}$, and Fe in Figure S10. We note that both methods of determining f_{LM} are in close agreement. For the hcp phases, adding 9 at% Ni to iron decreases f_{LM} by ∼1%. The f_{LM} of hcp-$Fe_{0.91}Ni_{0.09}$ and $Fe_{0.8}Ni_{0.1}Si_{0.1}$ are in close agreement, suggesting small amounts of silicon have a negligible effect on iron-nickel's f_{LM}. For the bcc-phases, the addition of nickel and silicon both decrease the f_{LM} of iron.

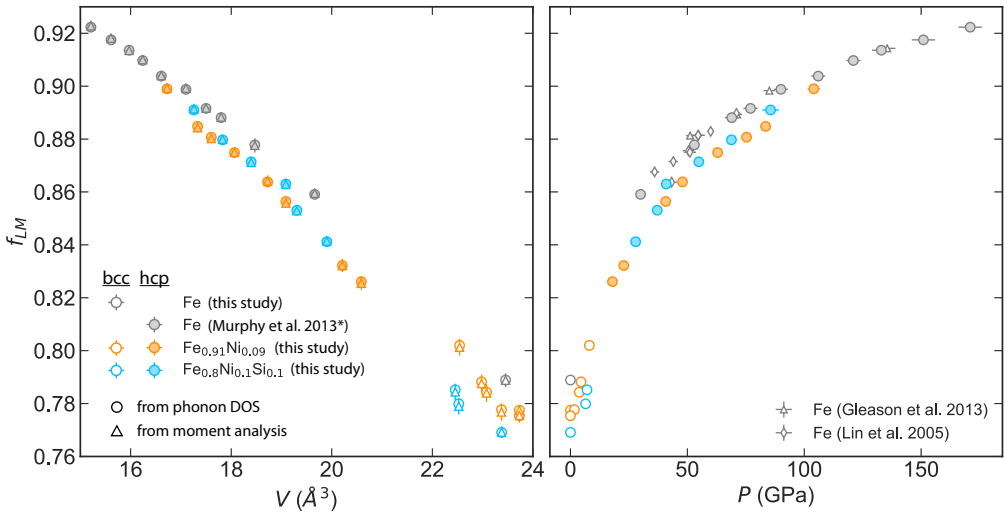

Figure S10: Left panel: f_{LM} for bcc- and hcp-$Fe_{0.91}Ni_{0.09}$, $Fe_{0.8}Ni_{0.1}Si_{0.1}$, and Fe calculated with a moments analysis of $S(E, V_i)$ (triangles) and determined from the phonon DOS (circles). (See text for more details.) The data for hcp-Fe is a re-analysis of data from *Murphy et al.* (2013). Error bars for f_{LM} from phonon DOS analysis are smaller than the displayed symbols. Right panel: f_{LM} phonon DOS analysis for bcc- and hcp-$Fe_{0.91}Ni_{0.09}$, $Fe_{0.8}Ni_{0.1}Si_{0.1}$, and Fe are compared to f_{LM} from existing hcp-Fe studies (*Gleason et al.*, 2013; *Lin et al.*, 2005).

5. Vibrational entropy and thermal expansion: Additional figure

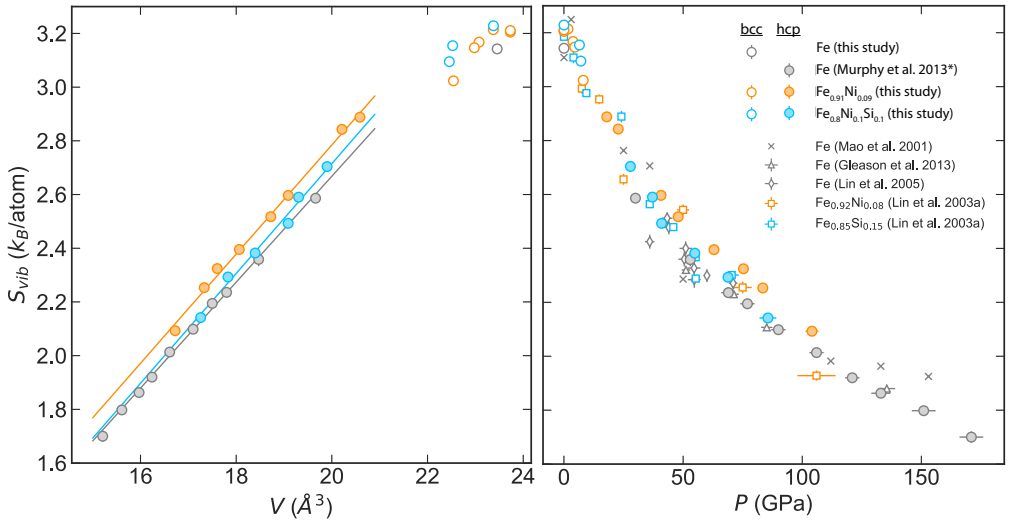

Figure S11: Vibrational harmonic component of entropy per ^{57}Fe resonant atom S_{vib} for bcc- and hcp-$Fe_{0.91}Ni_{0.09}$, $Fe_{0.8}Ni_{0.1}Si_{0.1}$, and Fe. The data for hcp-Fe is a re-analysis of data from *Murphy et al.* (2013). In the left panel, linear fits for the hcp phases are displayed. For hcp-Fe, we obtain a fit of $S_{vib} = 0.197V - 1.28$. For hcp-$Fe_{0.91}Ni_{0.09}$, $S_{vib} = 0.203V - 1.28$. For hcp-$Fe_{0.8}Ni_{0.1}Si_{0.1}$, $S_{vib} = 0.204V - 1.37$. In the right panel, we compare to S_{vib} from existing NRIXS studies: bcc- and hcp-Fe (*Mao et al.*, 2001; *Lin et al.*, 2005; *Gleason et al.*, 2013), $Fe_{0.92}Ni_{0.08}$, and $Fe_{0.85}Ni_{0.15}$ (*Lin et al.*, 2003).

6. Vibrational kinetic energy and specific heat capacity

The vibrational kinetic energy per ^{57}Fe resonant atom E_K at 300 K can be determined from NRIXS data in two ways. The first method uses the moment analysis of the excitation probability density $S(E, V_i)$ (see Section 2 in the main text), where E_K is related to the 2nd-order moment $S_2(E, V_i)$ (*Sturhahn and Chumakov*, 1999). The second method is from the phonon DOS determined with the quasi-harmonic approximation. The vibrational internal energy per ^{57}Fe atom U_{vib},

$$U_{vib}(V) = \frac{1}{2}\int E \coth\frac{\beta E}{2} D(E,V)dE, \tag{S6}$$

is composed of equal parts kinetic and potential energy, so $E_K = (1/2)U_{vib}$. We calculate E_K for $Fe_{0.91}Ni_{0.09}$, $Fe_{0.8}Ni_{0.1}Si_{0.1}$, and Fe with the moment analysis and from the phonon DOS and compare in Figure S12. The E_K from both methods agree closely within error bars. The E_K as determined with the phonon DOS is listed in Table S5. The difference between compositions for the bcc phases is negligible. For the hcp phases, the E_K of $Fe_{0.91}Ni_{0.09}$ trends slightly below those of $Fe_{0.8}Ni_{0.1}Si_{0.1}$ and Fe.

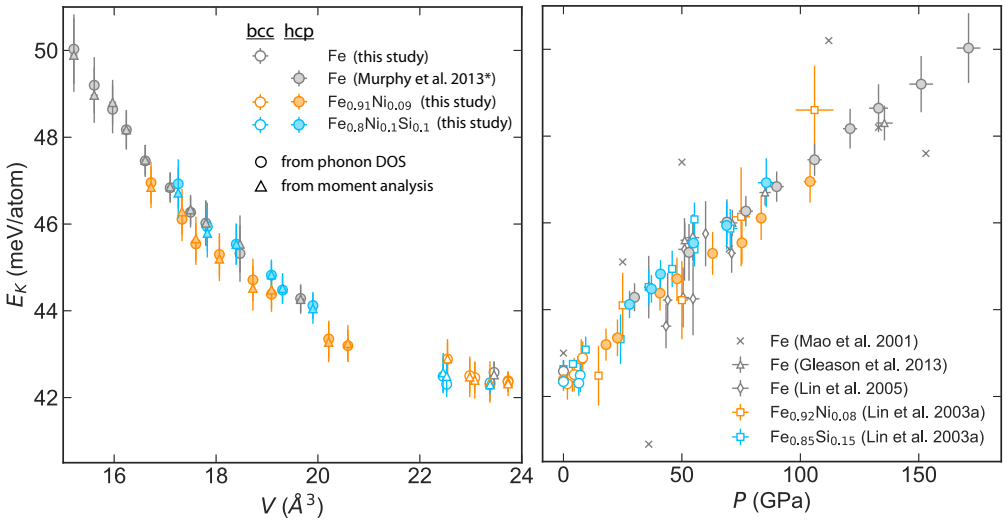

Figure S12: Left panel: Vibrational kinetic energy per ^{57}Fe atom E_K at 300 K for bcc- and hcp-$Fe_{0.91}Ni_{0.09}$, $Fe_{0.8}Ni_{0.1}Si_{0.1}$, and Fe calculated with a moments analysis of $S(E, V_i)$ (triangles) and from the phonon DOS (circles). (See text for more details.) The data for hcp-Fe is a re-analysis of data from *Murphy et al.* (2013). Right panel: E_K phonon DOS analysis for bcc- and hcp-$Fe_{0.91}Ni_{0.09}$, $Fe_{0.8}Ni_{0.1}Si_{0.1}$, and Fe are compared to other NRIXS studies: bcc- and hcp-Fe (*Mao et al.*, 2001; *Lin et al.*, 2005; *Gleason et al.*, 2013), $Fe_{0.92}Ni_{0.08}$, and $Fe_{0.85}Ni_{0.15}$ (*Lin et al.*, 2003).

Lastly, the phonon DOS also yields the vibrational component of the specific heat capacity via

$$C_{vib}(V) = k_B \int \left(\frac{\beta E}{2\sinh(\beta E/2)} \right)^2 D(E,V) dE. \tag{S7}$$

We plot the C_{vib} as a function of volume for bcc- and hcp-$Fe_{0.91}Ni_{0.09}$, $Fe_{0.8}Ni_{0.1}Si_{0.1}$, and Fe at 300 K in Figure S13 and listed in Table S5. The three hcp phases have similar trends with volume, with the C_{vib} of hcp-$Fe_{0.91}Ni_{0.09}$ falling slightly above those of $Fe_{0.8}Ni_{0.1}Si_{0.1}$ and Fe.

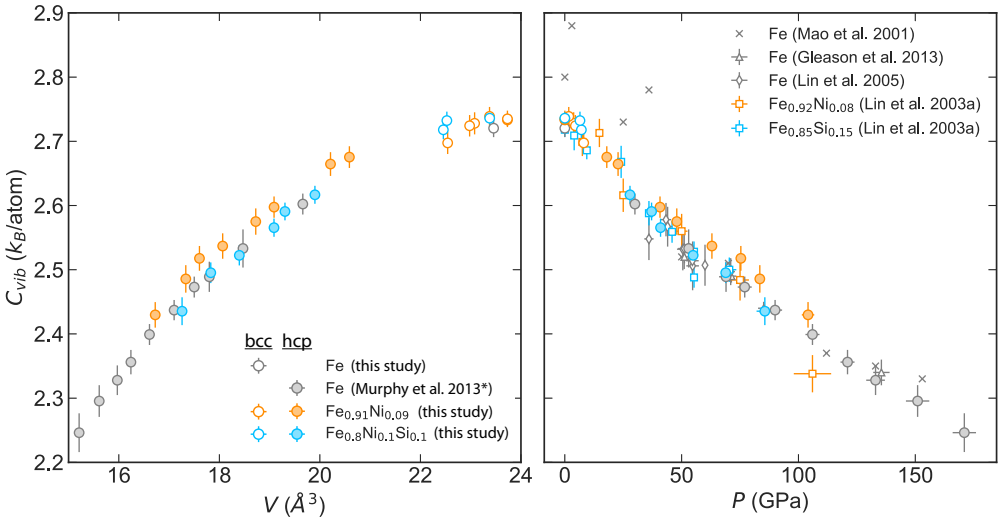

Figure S13: Left panel: Vibrational harmonic component of the specific heat capacity C_{vib} for bcc- and hcp-$Fe_{0.91}Ni_{0.09}$, $Fe_{0.8}Ni_{0.1}Si_{0.1}$, and Fe at 300 K. The data for hcp-Fe is a re-analysis of data from *Murphy et al.* (2013). Right panel: We compare our C_{vib} to existing studies: bcc- and hcp-Fe (*Mao et al.*, 2001; *Lin et al.*, 2005; *Gleason et al.*, 2013), $Fe_{0.92}Ni_{0.08}$, and $Fe_{0.85}Ni_{0.15}$ (*Lin et al.*, 2003).

7. Comparison of quantities reported in *Murphy et al.* (2013) and in this study

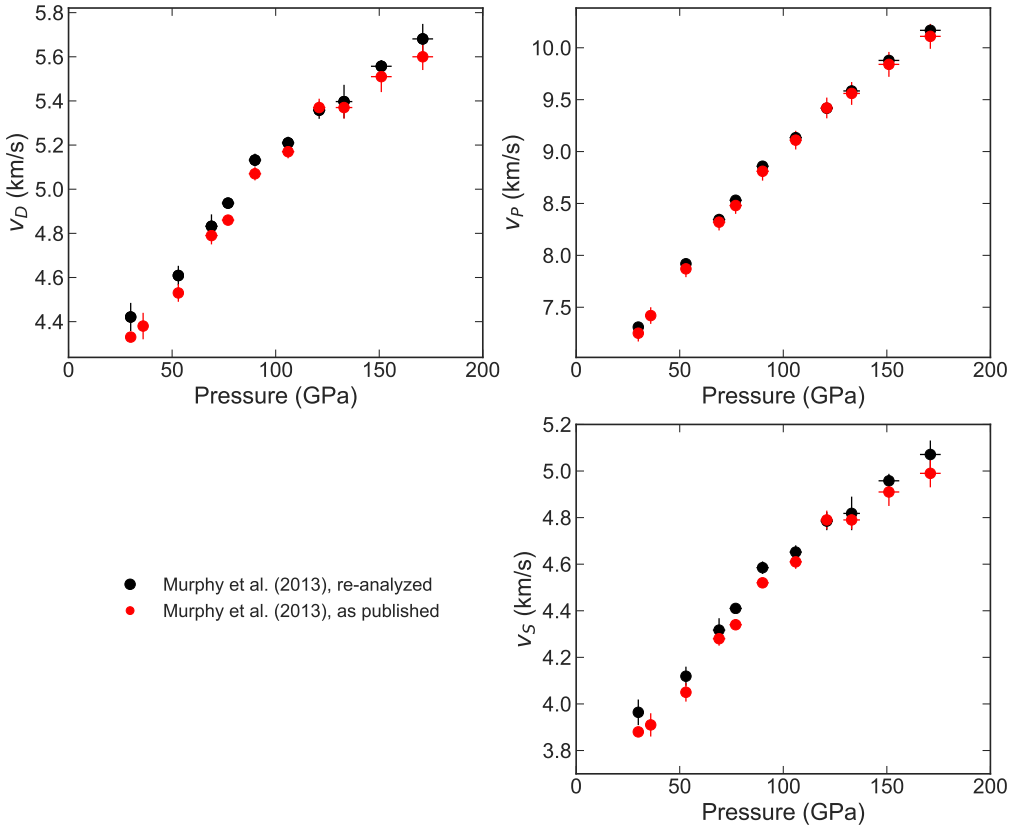

Figure S14: Comparison of hcp-Fe velocities at 300 K reported in *Murphy et al.* (2013) and our re-analysis using the same data set. We exclude the data point at 36 GPa, as we found the statistical quality to be inferior to the other scans in this study. Variations the resulting velocities arise from differences in the Debye velocity determination (see text for more details). The velocities presented here correspond to isotopically enriched samples (i.e., not yet corrected for natural isotopic enrichment).

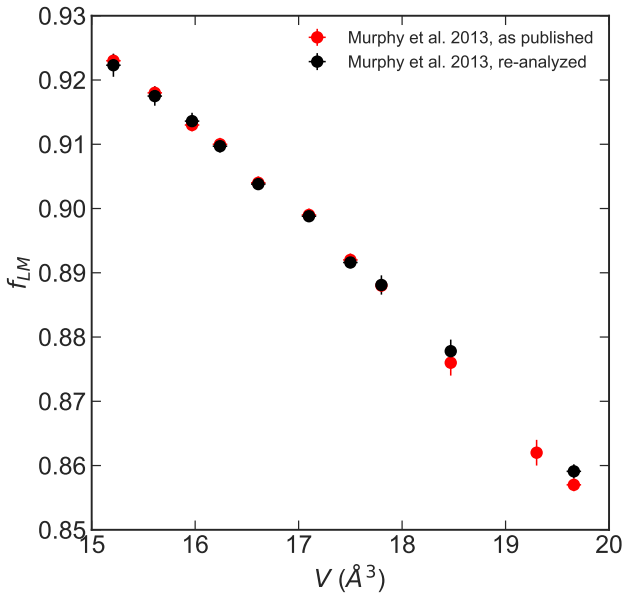

Figure S15: Comparison of hcp-Fe Lamb-Mössbauer factor at 300 K reported in *Murphy et al.* (2013) and our re-analysis using the same data set.

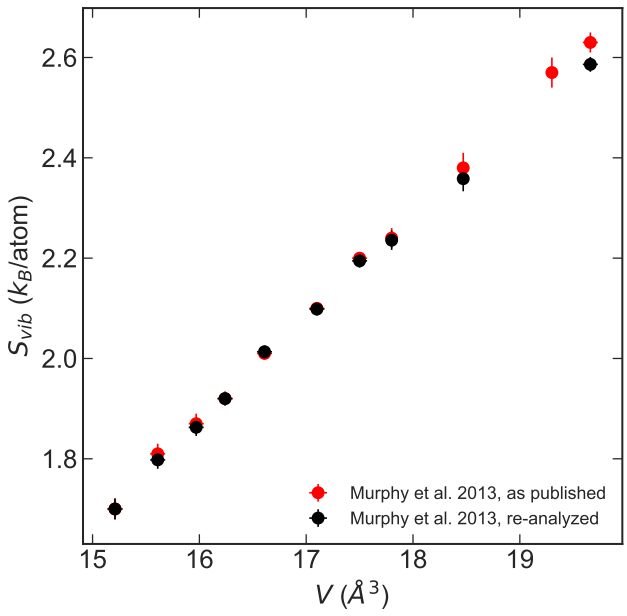

Figure S16: Comparison of hcp-Fe vibrational harmonic component of entropy at 300 K reported in *Murphy et al.* (2013) and our re-analysis using the same data set.

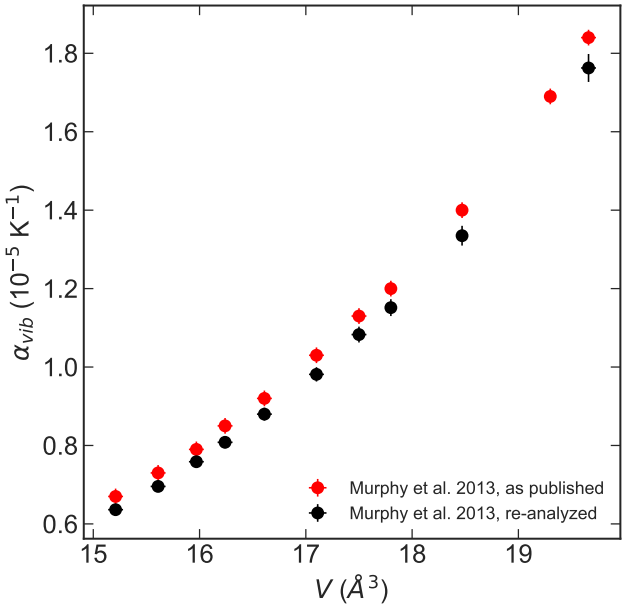

Figure S17: Comparison of hcp-Fe vibrational harmonic component of thermal expansion at 300 K reported in *Murphy et al.* (2013) and our re-analysis using the same data set.

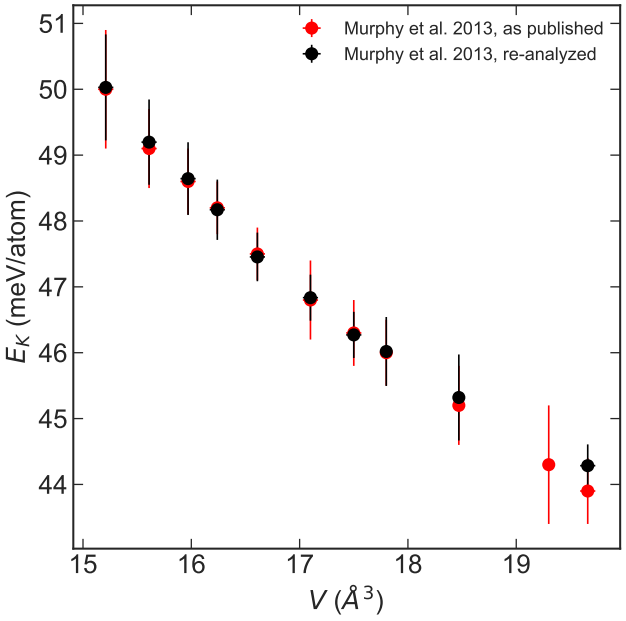

Figure S18: Comparison of hcp-Fe vibrational kinetic energy per ^{57}Fe atom at 300 K reported in *Murphy et al.* (2013) and our re-analysis using the same data set.

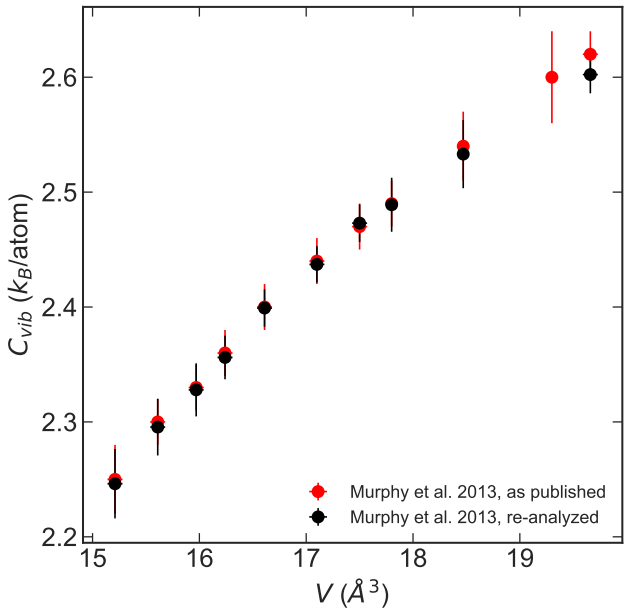

Figure S19: Comparison of hcp-Fe vibrational harmonic component of specific heat capacity at 300 K reported in *Murphy et al.* (2013) and our re-analysis using the same data set.

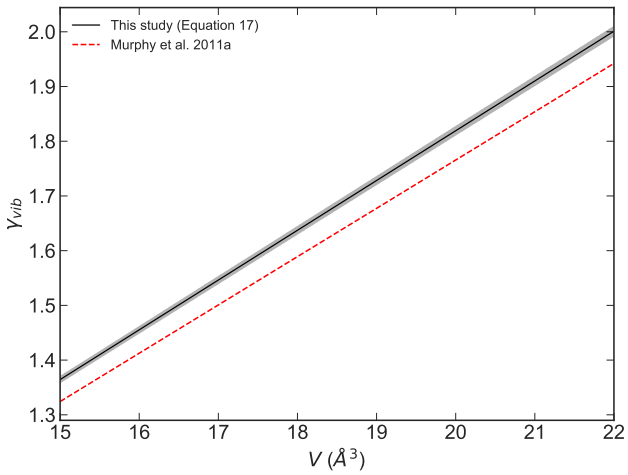

Figure S20: Comparison of hcp-Fe vibrational vibrational Grüneisen parameter at 300 K reported in *Murphy et al.* (2011a) and our re-analysis using the same data set. For both studies $q = 1$.

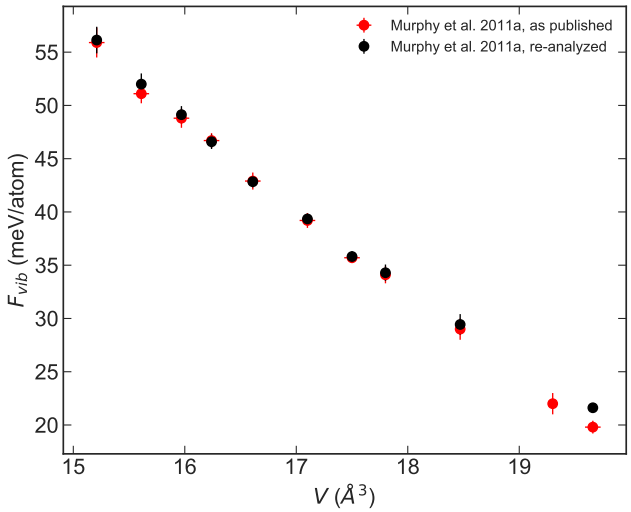

Figure S21: Comparison of hcp-Fe vibrational harmonic component of free energy at 300 K reported in *Murphy et al.* (2011a) and our re-analysis using the same data set.

8. Additional tables

Table S1: Experimental conditions for nuclear resonant scattering measurements

Run	Phase	P (GPa)	Energy range (meV)	Points per scan	Scan length (s/pt)	Number of scans
Fe						
Ambient	bcc	0	-80 to +90	681	5	2
$Fe_{0.91}Ni_{0.09}$						
Ambient	bcc	0	-80 to +90	681	11	4
FeNi-Run#1	bcc	1.7(1)	-80 to +100	721	55	11
		4.5(1)	-80 to +100	721	35	7
FeNi-Run#2	bcc	3.8(1)	-80 to +100	721	13	3
		8.1(1)	-80 to +100	721	23	4
	hcp	18.0(1)	-70 to +100	681	20	4
		22.8(2)	-70 to +100	681	18	4
		41(1)	-70 to +100	681	30	6
		48(1)	-70 to +100	681	25	5
		63(1)	-70 to +100	681	38	8
		75(1)	-70 to +100	681	38	8
		83(1)	-70 to +100	681	30	7
		104(3)	-70 to +100	681	35	9
$Fe_{0.8}Ni_{0.1}Si_{0.1}$						
Ambient	bcc	0	-80 to +100	681	6	2
FeNiSi-Run#1	bcc	7.1(1)	-80 to +110	761	36	8
FeNiSi-Run#2	bcc	6.5(1)	-80 to +100	721	39	12
FeNiSi-Run#3	hcp	27.9(3)	-80 to +100	721	39	12
		37.1(6)	-80 to +100	721	48	12
		41(1)	-80 to +100	721	56	20
		55(1)	-80 to +100	721	63	21
		69(1)	-80 to +100	721	61	23
		86(3)	-80 to +100	721	60	23

Table S2: Equation of state parameters and experimental conditions

Phase	V_0 (Å^3)	K_0 (GPa)	K_0'	P range (GPa)	P medium	P gauge[d]	EOS
bcc-Fe[a]	23.524(18)	168.1(8.3)	4.7(1.3)	0-14.6	He	W, ruby	Vinet
bcc-$Fe_{0.91}Ni_{0.09}$[b]	23.635(6)	146.7(3.0)	6.42(60)	0-15.2	He	W	Vinet
bcc-$Fe_{0.8}Ni_{0.1}Si_{0.1}$[b]	23.385(9)	155.6(7.4)	5.7(1.2)	0-21.6	He	W	Vinet
hcp-Fe[c]	22.428(98)	163.4(7.9)	5.38(16)	17-197	He	W, ruby	Vinet
hcp-$Fe_{0.91}Ni_{0.09}$[b]	22.505(42)	157.5(3.9)	5.61(10)	14.6-167	He	W	Vinet
hcp-$Fe_{0.8}Ni_{0.1}Si_{0.1}$[b]	22.952(72)	125.2(4.6)	6.38(12)	21.6-175	He	W	Vinet
hcp-$Fe_{0.868}Ni_{0.086}Si_{0.046}$[e]	22.6(2)	170(6)	4.8(2)	20–147	Ne	Pt	3BM[f]

[a] *Morrison et al.* (2018) after data from *Dewaele et al.* (2006)
[b] *Morrison et al.* (2018)
[c] *Dewaele et al.* (2006)
[d] All listed equations of state use pressure gauges from *Dorogokupets and Oganov* (2006)
[e] *Liu et al.* (2016)
[f] Third order Birch-Murnaghan

Table S3: Natural and enriched molecular masses M of samples

Composition	M_{enr}[a] (g/mol)	M_{nat}[b] (g/mol)
Fe	56.942	55.845
$Fe_{0.91}Ni_{0.09}$	57.100	56.101
$Fe_{0.8}Ni_{0.1}Si_{0.1}$	54.231	53.354

[a] Fe 95% enriched in ^{57}Fe
[b] Fe with natural isotopic enrichment

Table S4: Sound velocity analysis results with density and velocities corrected for natural enrichment

V (Å^3)	ρ (g/cm^3)	P (GPa)	v_D (km/s)	v_P (km/s)	v_S (km/s)
bcc-Fe					
23.46(3)	7.91(1)	0	3.50(3)	5.87(9)	3.14(3)
hcp-Fe[a]					
19.66(7)	9.42(3)	30(2)	4.46(6)	7.38(5)	4.00(6)
18.47(3)	10.05(1)	53(2)	4.65(4)	8.00(3)	4.16(4)
17.80(3)	10.43(1)	69(3)	4.88(5)	8.43(4)	4.36(5)
17.50(7)	10.59(2)	77(3)	4.99(2)	8.61(2)	4.45(2)
17.10(7)	10.85(2)	90(3)	5.18(3)	8.95(2)	4.63(3)
16.61(7)	11.16(5)	106(3)	5.26(3)	9.22(3)	4.70(3)
16.24(7)	11.42(2)	121(3)	5.41(4)	9.51(3)	4.83(4)
15.97(7)	11.61(2)	133(4)	5.45(8)	9.68(5)	4.87(7)
15.61(7)	11.90(3)	151(5)	5.61(3)	9.97(3)	5.01(3)
15.21(7)	12.19(3)	171(5)	5.74(7)	10.27(4)	5.12(6)
bcc-$Fe_{0.91}Ni_{0.09}$					
23.73(2)	7.85(1)	0	3.30(2)	5.51(4)	2.95(2)
23.38(3)	7.97(1)	1.7(1)	3.31(2)	5.61(3)	2.96(2)
23.08(3)	8.07(1)	3.8(1)	3.34(2)	5.74(2)	2.98(2)
22.98(3)	8.11(1)	4.5(1)	3.42(2)	5.83(2)	3.06(2)
22.54(2)	8.26(1)	8.1(1)	3.49(1)	6.06(2)	3.12(1)
hcp-$Fe_{0.91}Ni_{0.09}$					
20.59(2)	9.05(1)	18.0(1)	3.88(5)	6.64(4)	3.46(5)
20.21(3)	9.22(1)	22.8(2)	3.97(3)	6.85(3)	3.55(3)
19.09(6)	9.76(3)	41(1)	4.28(1)	7.50(1)	3.82(1)
18.72(4)	9.95(2)	48(1)	4.40(4)	7.74(2)	3.92(3)
18.07(4)	10.31(2)	63(1)	4.56(3)	8.14(2)	4.06(2)
17.60(2)	10.58(1)	75(1)	4.64(2)	8.41(1)	4.13(2)
17.33(3)	10.75(2)	83(1)	4.71(4)	8.59(3)	4.20(3)
16.72(4)	11.14(3)	104(3)	5.02(4)	9.09(3)	4.47(3)
bcc-$Fe_{0.8}Ni_{0.1}Si_{0.1}$					
23.38(3)	7.58(1)	0	3.23(1)	5.63(9)	2.89(1)
22.53(3)	7.87(1)	6.5(1)	3.26(3)	5.96(3)	2.90(3)
22.46(2)	7.89(1)	7.1(1)	3.28(3)	6.00(3)	2.92(3)
hcp-$Fe_{0.8}Ni_{0.1}Si_{0.1}$					
19.90(3)	8.90(2)	27.9(3)	4.00(5)	7.00(3)	3.57(4)
19.31(5)	9.18(2)	37.1(6)	4.19(4)	7.38(3)	3.73(3)
19.09(6)	9.28(3)	41(1)	4.34(5)	7.59(4)	3.87(5)
18.40(5)	9.63(2)	55(1)	4.41(4)	7.98(3)	3.93(4)
17.83(4)	9.94(2)	69(1)	4.58(6)	8.40(4)	4.08(5)
17.26(6)	10.27(4)	86(3)	4.72(4)	8.81(3)	4.20(4)

[a]Re-analyzed from *Murphy et al.* (2013)

Table S5: Additional vibrational quantities derived from the phonon DOS

Phase	V (Å^3)	P (GPa)	f_{LM}	S_{vib} (k_B/atom)	α_{vib} (10^{-5}K^{-1})	E_K (meV/atom)	C_{vib} (k_B/atom)
bcc-Fe							
	23.46(3)	0	0.789(1)	3.14(1)		14.2(1)	2.72(1)
hcp-Fe							
	19.66(7)	30(2)	0.859(1)	2.59(1)	1.76(4)	14.8(1)	2.60(2)
	18.47(3)	53(2)	0.878(2)	2.36(3)	1.33(3)	15.1(2)	2.53(3)
	17.80(3)	69(3)	0.888(2)	2.24(2)	1.15(2)	15.3(2)	2.49(2)
	17.50(7)	77(3)	0.892(1)	2.19(1)	1.08(2)	15.4(1)	2.47(2)
	17.10(7)	90(3)	0.899(1)	2.10(1)	0.98(2)	15.6(1)	2.44(2)
	16.61(7)	106(3)	0.904(1)	2.01(1)	0.88(2)	15.8(1)	2.40(2)
	16.24(7)	121(3)	0.910(1)	1.92(1)	0.81(2)	16.1(2)	2.36(2)
	15.97(7)	133(4)	0.914(1)	1.86(2)	0.76(1)	16.2(2)	2.33(2)
	15.61(7)	151(5)	0.918(2)	1.80(2)	0.70(1)	16.4(2)	2.30(2)
	15.21(7)	171(5)	0.922(2)	1.70(2)	0.64(1)	16.7(3)	2.25(3)
bcc-$Fe_{0.91}Ni_{0.09}$							
	23.73(2)	0	0.775(1)	3.21(1)		14.1(1)	2.74(1)
	23.38(3)	1.7(1)	0.778(2)	3.21(2)		14.1(1)	2.74(1)
	23.08(3)	3.8(1)	0.784(2)	3.17(2)		14.2(1)	2.73(2)
	22.98(3)	4.5(1)	0.788(2)	3.15(2)		14.2(1)	2.72(2)
	22.54(2)	8.1(1)	0.802(2)	3.02(2)		14.3(1)	2.70(2)
hcp-$Fe_{0.91}Ni_{0.09}$							
	20.59(2)	18.0(1)	0.826(1)	2.89(2)	2.24(5)	14.4(1)	2.68(2)
	20.21(3)	22.8(2)	0.832(1)	2.84(2)	2.05(4)	14.5(1)	2.66(2)
	19.09(6)	41(1)	0.856(1)	2.60(2)	1.57(3)	14.8(1)	2.60(2)
	18.72(4)	48(1)	0.864(1)	2.52(2)	1.45(3)	14.9(2)	2.58(2)
	18.07(4)	63(1)	0.875(1)	2.40(2)	1.24(2)	15.1(2)	2.54(2)
	17.60(2)	75(1)	0.881(1)	2.32(2)	1.11(2)	15.2(2)	2.52(2)
	17.33(3)	83(1)	0.885(1)	2.25(2)	1.04(2)	15.4(2)	2.49(2)
	16.72(4)	104(3)	0.899(1)	2.09(2)	0.91(2)	15.7(2)	2.43(2)
bcc-$Fe_{0.8}Ni_{0.1}Si_{0.1}$							
	23.38(3)	0	0.769(1)	3.23(1)		14.1(1)	2.74(1)
	22.53(3)	6.5(1)	0.780(2)	3.15(1)		14.1(1)	2.73(1)
	22.46(2)	7.1(1)	0.785(2)	3.09(1)		14.2(1)	2.72(1)
hcp-$Fe_{0.8}Ni_{0.1}Si_{0.1}$							
	19.90(3)	27.9(3)	0.841(1)	2.70(1)	2.01(4)	14.7(1)	2.62(1)
	19.31(5)	37.1(6)	0.853(1)	2.59(1)	1.72(3)	14.8(1)	2.59(1)
	19.09(6)	41(1)	0.863(1)	2.49(1)	1.63(3)	14.9(1)	2.57(1)
	18.40(5)	55(1)	0.871(1)	2.38(1)	1.37(2)	15.2(2)	2.52(2)
	17.83(4)	69(1)	0.880(1)	2.29(1)	1.18(2)	15.3(2)	2.50(2)
	17.26(6)	86(3)	0.891(1)	2.14(2)	1.02(2)	15.6(2)	2.44(2)

[a] Re-analyzed from *Murphy et al.* (2011b)

References

Dewaele, A., P. Loubeyre, F. Occelli, M. Mezouar, P. Dorogokupets, and M. Torrent (2006), Quasihydrostatic equation of state of iron above 2 Mbar, *Physical Review Letters*, *97*, 215,504, doi:10.1103/PhysRevLett.97.215504.

Dorogokupets, P. I., and A. R. Oganov (2006), Equations of state of Al, Au, Cu, Pt, Ta, and W and revised ruby pressure scale, *Doklady Earth Sciences*, *410*(1), 1091–1095, doi:10.1134/S1028334X06070208.

Fei, Y., C. Murphy, Y. Shibazaki, A. Shahar, and H. Huang (2016), Thermal equation of state of hcp-iron: Constraint on the density deficit of Earth's solid inner core, *Geophysical Research Letters*, *43*, 6837–6843, doi:10.1002/2016GL069456.

Gleason, A. E., W. L. Mao, and J. Y. Zhao (2013), Sound velocities for hcp-iron compressed hydrostatically to 136 GPa from phonon density of states, *Geophysical Research Letters*, *40*, 2983–2987, doi:10.1002/grl.50588.

Lin, J.-F., V. V. Struzhkin, W. Sturhahn, E. Huang, J. Zhao, M. Y. Hu, E. E. Alp, H.-k. Mao, N. Boctor, and R. J. Hemley (2003), Sound velocities of iron-nickel and iron-silicon alloys at high pressures, *Geophysical Research Letters*, *30*(21), 2112, doi:10.1029/2003GL018405.

Lin, J.-F., W. Sturhahn, J. Zhao, G. Shen, H.-K. Mao, and R. J. Hemley (2005), Sound velocities of hot dense iron: Birch's law revisited, *Science*, *308*, 1892–1894, doi:10.1126/science.1111724.

Liu, J., J.-F. Lin, A. Alatas, A. Alatas, M. Y. Hu, J. Zhao, and L. Dubrovinsky (2016), Seismic parameters of hcp-Fe alloyed with Ni and Si in the Earth's Core, *Journal of Geophysical Research: Solid Earth*, *121*, doi:10.1002/2015JB012625.

Mao, H. K., J. Xu, V. V. Struzhkin, J. Shu, R. J. Hemley, W. Sturhahn, M. Y. Hu, E. E. Alp, L. Vocadlo, D. Alfè, G. D. Price, M. J. Gillan, M. Schwoerer-Böhning, D. Häusermann, P. Eng, G. Shen, H. Giefers, R. Lübbers, and G. Wortmann (2001), Phonon density of states of iron up to 153 gigapascals, *Science*, *292*(914), 914–6, doi:10.1126/science.1057670.

Morrison, R. A., J. M. Jackson, W. Sturhahn, D. Zhang, and E. Greenberg (2018), Equations of state and anisotropy of Fe-Ni-Si alloys, *Journal of Geophysical Research: Solid Earth*, *123*, doi:10.1029/2017JB015343.

Murphy, C. A., J. M. Jackson, W. Sturhahn, and B. Chen (2011a), Grüneisen parameter of hcp-Fe to 171 GPa, *Geophysical Research Letters*, *38*(24), 1–5, doi:10.1029/2011GL049531.

Murphy, C. A., J. M. Jackson, W. Sturhahn, and B. Chen (2011b), Melting and thermal pressure of hcp-Fe from the phonon density of states, *Physics of the Earth and Planetary Interiors*, *188*, 114–120, doi:10.1016/j.pepi.2011.07.001.

Murphy, C. A., J. M. Jackson, and W. Sturhahn (2013), Experimental constraints on the thermodynamics and sound velocities of hcp-Fe to core pressures, *Journal of Geophysical Research: Solid Earth*, *118*, doi:10.1002/jgrb.50166.

Sturhahn, W. (2004), Nuclear resonant spectroscopy, *Journal of Physics: Condensed Matter*, *16*(5), S497–S530, doi:10.1088/0953-8984/16/5/009.

Sturhahn, W., and A. Chumakov (1999), Lamb-Mössbauer factor and second-order Doppler shift from inelastic nuclear resonant absorption, *Hyperfine Interactions*, *123/124*, 809–824, doi:10.1023/A:1017060931.